# Navigation System Fault Diagnosis for Underwater Vehicle

**Thomas Falkenberg** [*] **René Tavs Gregersen** [*]
**Mogens Blanke** [*,**]

[*] *Automation and Control Group, Department of Electrical
Engineering, Technical University of Denmark, Kgs. Lyngby, Denmark
e-mail: mb@elektro.dtu.dk*
[**] *AMOS Centre of Excellence, Institute for Technical Cybernetics,
Norwegian University of Science and Technology, Trondheim, Norway*

**Abstract:** This paper demonstrates fault diagnosis on unmanned underwater vehicles (UUV) based on analysis of structure of the nonlinear dynamics. Residuals are generated using different approaches in structural analysis followed by statistical change detection. Hypothesis testing thresholds are made signal based to cope with non-ideal properties seen in real data. Detection of both sensor and thruster failures are demonstrated. Isolation is performed using the residual signature of detected faults and the change detection algorithm is used to assess severity of faults by estimating their magnitude. Numerical simulations and sea trial data show results with very favourable balance between detection and false alarm probabilities. ©IFAC 2014.

## 1. INTRODUCTION

Unmanned Underwater Vehicles (UUVs) are useful and important tools for accomplishing a great variety of underwater tasks ranging from scientific investigation of marine life and environment to underwater archaeology survey, repair and maintenance of subsea structures. Some of the main dangers to UUVs are failures of thrusters and sensors. These can have significant effects on the behaviour and manoeuvrability of a UUV, possibly proving fatal in hazardous or difficult to reach locations [Griffiths and Trembanis, 2007]. It is thus desirable to apply fault diagnosis as a first step to accommodating faults. Several different methods have been applied on UUVs for fault detection (see also the early survey [Antonelli, 2006]): observer-based [Alessandri et al., 1999, Ferreira et al., 2011]; fuzzy logic [Omerdic and Roberts, 2004]; neural network [Liu et al., 2012] and structural analysis based methods [Blanke, 2005]. Actuator failures were in specific focus in [Corradini et al., 2011],and with an observer based fault tolerant control approach tested in simulation in [Corradini and Orlando, 2014], but vessel-wide navigation system diagnosis has not been reported.

This paper employs a structural analysis based design of a fault diagnosis scheme for the entire sensor and actuator package of the underwater Remotely Operated Vehicle (ROV) Minerva, depicted in Fig. 1. Fault isolation properties are investigated using different methods to obtain the analytical redundancy relations needed for diagnosis, and statistical change detection [Blanke et al., 2006] is demonstrated on both simulated and real data. It is shown how fault isolation is obtained with prescribed false alarm and detection probabilities. The paper contributes with a complete navigation system analysis based on component behaviours and the tailoring of statistical change detection methods to obtain excellent diagnostic properties also with

real data, where signal artifacts include outliers and time-varying coloured noise.

The paper first introduces the specific configuration of the ROV, it is then detailed how complete analysis of all analytic redundancy relations are obtained, and how these are optimised for maximal fault isolability. Change detection is then considered and the diagnosis scheme is applied on both simulation and real data.



Fig. 1. ROV Minerva [1], a SUB-fighter 7500 ROV from Sperre A/S. Photo: Johanna Järnegren

## 2. MATHEMATICAL MODEL

The vessel is modelled using the kinematic and dynamics of a 4 degree of freedom underwater vehicle as described in Fossen [2002]. It is actuated in surge, sway, heave and yaw. With vessel's position and heading $\boldsymbol{\eta} = [x \ y \ z \ \psi]^T$ in an inertial frame and the velocities and turn rate $\boldsymbol{\nu} = [u \ v \ w \ r]^T$ in a body frame, the kinematics are given in (1),

$$\dot{\boldsymbol{\eta}} = \mathbf{J}(\boldsymbol{\eta})\boldsymbol{\nu}, \tag{1}$$

---

[1]  Courtesy of NTNU (*http://www.ntnu.edu/marine/minerva*)

where

$$\mathbf{J}(\boldsymbol{\eta}) = \begin{bmatrix} \cos\psi & -\sin\psi & 0 & 0 \\ \sin\psi & \cos\psi & 0 & 0 \\ 0 & 0 & 1 & 0 \\ 0 & 0 & 0 & 1 \end{bmatrix}.$$

The vessel is passively stable in roll and pitch so these motions are disregarded. With $\boldsymbol{\nu}_c = [u_c, v_c, w_c, 0]$ denoting sea current velocity, assumed to be slowly varying and irrotational, and the relative velocity defined as $\boldsymbol{\nu}_r = \boldsymbol{\nu} - \boldsymbol{\nu}_c$ the vessel dynamics reads,

$$\mathbf{M}_{RB}\dot{\boldsymbol{\nu}} + \mathbf{M}_A\dot{\boldsymbol{\nu}}_r + \mathbf{C}_{RB}(\boldsymbol{\nu})\boldsymbol{\nu} + \mathbf{C}_A(\boldsymbol{\nu}_r)\boldsymbol{\nu}_r$$
$$+ \mathbf{D}(\boldsymbol{\nu}_r)\boldsymbol{\nu}_r + \mathbf{g}(\boldsymbol{\eta}) = \boldsymbol{\tau} + \mathbf{w}, \qquad (2)$$

where $\mathbf{M}_{RB}$, $\mathbf{M}_A \in \mathbb{R}^{4\times4}$ are the rigid-body and added mass system inertia matrices respectively, $\mathbf{C}_{RB}(\boldsymbol{\nu})$, $\mathbf{C}_A(\boldsymbol{\nu})$ $\in \mathbb{R}^{4\times4}$ are the corresponding coriolis-centripetal matrices, $\mathbf{D}(\boldsymbol{\nu}) \in \mathbb{R}^{4\times4}$ is a damping matrix, $\mathbf{g}(\boldsymbol{\eta}) \in \mathbb{R}^4$ is a vector of restoring forces, $\boldsymbol{\tau} \in \mathbb{R}^4$ is the vector of forces induced by vehicle thrusters, and $\mathbf{w} \in \mathbb{R}^4$ is a vector of environmental disturbances. See [Fossen, 2011] concerning the generic model (2) and [Kirkeby, 2010] for numerical values for Minerva.

The ocean current observer described in [Børhaug et al., 2007] is used in this paper. This is a constant-gain non-linear observer in the 6 degrees of freedom, however only the 4 relevant degrees of freedom are utilized in this project. This was shown to be UGAS to a constant current [Børhaug et al., 2007].

The available measurements on Minerva are positions $\{x_m, y_m, z_m\}$, heading $\phi_m$ and rates $\{u_m, v_m, r_m\}$, see [Kirkeby, 2010] for a sensor suite description.

The vessel has 5 fixed direction thrusters [2] providing the thrust according to (3),

$$\boldsymbol{\tau} = \mathbf{TKu}, \qquad (3)$$

where $\mathbf{T} \in \mathbb{R}^{4\times4}$ is the thruster configuration matrix, $\mathbf{K} \in \mathbb{R}^{4\times4}$ is a thrust coefficient matrix describing the thruster characteristics and $\mathbf{u} \in \mathbb{R}^4$ is the control input, see Fig. 2. $\mathbf{T}$ is given in (4)

$$\mathbf{T} = \begin{bmatrix} c(\alpha_p) & s(\alpha_s) & 0 & 0 \\ s(\alpha_p) & c(\alpha_s) & 1 & 0 \\ 0 & 0 & 0 & 2 \\ x_p s(\alpha_p) - y_p c(\alpha_p) & x_s s(\alpha_s) - y_s c(\alpha_s) & x_{lat} & 0 \end{bmatrix}, \quad (4)$$

where the distances $x_p$, $y_p$, $x_s$, $y_s$ and $x_{lat}$ correspond to the schematic on Fig. 2, $c$, $s$ are cos() and sin() functions respectively and $\alpha_p$ and $\alpha_s$ are the angles of the thrusters in relation to the $x_b$ axis.

The details of control systems for Minerva was presented in [Dukan et al., 2011, Sørensen et al., 2012]. When the control objective is dynamic positioning, i.e the goal is to keep $\tilde{\boldsymbol{\eta}} = \boldsymbol{\eta}_d - \boldsymbol{\eta} = 0$, where $\boldsymbol{\eta}_d$ is the desired position, a non-linear PID controller, was used:

$$\boldsymbol{\tau}_{con} = -\mathbf{J}^T(\boldsymbol{\eta})\left(\mathbf{K}_p\tilde{\boldsymbol{\eta}} + \mathbf{K}_d\boldsymbol{\nu} + \mathbf{K}_i\int_0^T\tilde{\boldsymbol{\eta}}(t)dt\right) \qquad (5)$$

$$\mathbf{u} = \mathbf{K}^{-1}\mathbf{T}^\dagger\boldsymbol{\tau}_{con}, \qquad (6)$$

---

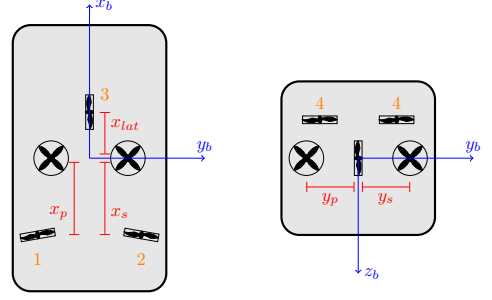[2] The two vertical thrusters are coupled to the same control signal hence effectively operating as one.



Fig. 2. Minerva schematic. Blue lines indicate coordinate axes in the b-frame. Red lines show thruster offsets.

where $\mathbf{K}_p, \mathbf{K}_d, \mathbf{K}_i \in \mathbb{R}^{4\times4}$ are the controller gains and $\mathbf{T}^\dagger$ the Moore-Penrose pseudo inverse of $\mathbf{T}$. The coefficients in $\mathbf{K}$ of the controller in (5) were provided in [Kirkeby, 2010].

## 3. RESIDUAL GENERATION THROUGH STRUCTURAL ANALYSIS

Structural analysis [Blanke et al., 2006] and references herein is a graph-based method where only the structure of the system is considered and not the specific relationships between variables and parameters. Achieving system structure includes first to formulate normal behaviours through *constraints* between physical variables of the system. Constraints can be dynamic, e.g. differential equations, or they can be algebraic relations between variables. Constraints can be linear or nonlinear.

Described a *structural model* as a *bi-partite graph* where one set of vertices are the constraints $\mathcal{C}$, the other the variables $\mathcal{Z}$. Edges in the graph will show which variables are used by which constraints. The set of variables, denoted $\mathcal{Z}$, contains both known (i.e. inputs and measurements), denoted $\mathcal{K}$, and unknown variables, $\mathcal{X}$. One constraint is used to solve for one unknown variable. This list is referred to as a *matching*. With $|X|$ unknown variables, $|X|$ constraints are used to solve for unknown variables. Constraints that are not matched are redundant and express information that can be used to test the consistency of the system. The un-matched constraints hence constitute analytical redundancy relations that are used for fault diagnosis.

With no faults, all un-matched constraints are zero,

$$c^i_{arr}(x, u, y, \theta) = 0. \qquad (7)$$

As unknown variables were solved for through a complete matching, $x$ can be eliminated from (7),

$$c^i_{arr}(u, \dot{u}, \ddot{u}, \ldots, y, \dot{y}, \ddot{y}, \ldots, \theta) = 0, \qquad (8)$$

which is a function of only known variables and their derivatives. All constraints that were used to eliminate $x$ in $c^i_{arr}$ must meet their normal behaviour in order to have $c^i_{arr} = 0$. If any of the constraints used to calculate $c^i_{arr}$ deviate from normal behaviour, $c^i_{arr} \neq 0$. Structural analysis hence generates a set of analytical relations, referred to as residuals,

$$r^i(t) = c^i_{arr}(u(t), \dot{u}(t), \ddot{u}(t), \ldots, y(t), \dot{y}(t), \ddot{y}(t), \ldots, \theta). \qquad (9)$$

The analytical redundancies in (9) are easily determined from graph theory results, either in form of finding complete matchings on unknown variables [Blanke et al., 2006]

and references herein, or by finding minimal structurally over-determined sets [Krysander et al., 2008]. For the structural analysis described in this paper the SaTool software was used [Blanke and Lorentzen, 2006], [Wolf and Blanke, 2014].

Once the analytical form of residuals are determined according to (9), change detection methods and hypothesis testing are employed to determine whether the condition is normal $\mathcal{H}_0 : r(t) = 0$ or a fault is present, $\mathcal{H}_1 : r(t) \neq 0$. When residuals suffer from random noise $w(t)$, and if a certain fault manifests itself as a change in mean of the residual, from 0 to $\mu_1$, two hypotheses need be distinguished,

$$\mathcal{H}_0 : r(t) = \quad w(t) \tag{10}$$
$$\mathcal{H}_1 : r(t) = \mu_1 + w(t),$$

Residual evaluation and the hypothesis test according to (10) constitute the on-line part of the diagnosis. Analysis of structure and calculation of residuals to be used for diagnosis are part of supervision and control system design.

### 3.1 Behavioral model for Minerva ROV

The following constraints describe the Minerva ROV,

- 37 constraints as listed in Table 1.
- 14 known variables $\mathcal{K} = [\ u_1,\ u_2,\ u_3,\ u_4,\ x_m,\ y_m,\ z_m,$ $\psi_m,\ u_m,\ v_m,\ r_m,\ u_{c,m},\ v_{c,m},\ w_{c,m}\ ]$.
- 30 unknown variables $\mathcal{X} = [\ \tau_1,\ \tau_2,\ \tau_3,\ \tau_4,\ X,\ Y,\ Z,$ $N,\ \dot{x},\ \dot{y},\ \dot{z},\ \dot{\psi},\ \dot{u},\ \dot{v},\ \dot{w},\ \dot{r},\ x,\ y,\ z,\ u,\ v,\ w,\ \psi,\ r,\ u_c,\ v_c,$ $w_c,\ \dot{u}_c,\ \dot{v}_c,\ \dot{w}_c\ ]$,

where the subscript $m$ on the variables designate measurements, $\tau_{1-4}$ designate the force from the thrusters ($\tau_4$ corresponds to both vertical thruster as they can not be individually controlled), $X, Y, Z, N$ are the vessel force and moment in surge, sway heave and yaw respectively. Velocities with the subscript $c$ describe the ocean current affecting the vessel.

The Minerva system has 37 constraints and 30 unknown variables, hence it is over-constrained and 7 redundancy relations or residuals will be produced by using the ranking algorithm described in [Blanke et al., 2006]. These are shown in (11).

$$\begin{pmatrix} r_1 \\ r_2 \\ r_3 \\ r_4 \\ r_5 \\ r_6 \\ r_7 \end{pmatrix} \leftarrow \begin{array}{c} \begin{array}{ccccccccccc} u_1 & u_2 & u_3 & u_4 & x_m & y_m & z_m & \psi_m & u_m & v_m & r_m \end{array} \\ \begin{pmatrix} 0 & 0 & 0 & 0 & 1 & 0 & 0 & 1 & 1 & 1 & 0 \\ 0 & 0 & 0 & 0 & 0 & 1 & 0 & 1 & 1 & 1 & 0 \\ 0 & 0 & 0 & 0 & 0 & 0 & 0 & 1 & 0 & 0 & 1 \\ 0 & 0 & 0 & 1 & 0 & 0 & 1 & 0 & 0 & 0 & 0 \\ 1 & 1 & 0 & 0 & 0 & 0 & 0 & 0 & 1 & 1 & 1 \\ 1 & 1 & 1 & 0 & 0 & 0 & 0 & 0 & 1 & 1 & 1 \\ 1 & 1 & 1 & 0 & 0 & 0 & 0 & 0 & 1 & 1 & 1 \end{pmatrix} \end{array} \tag{11}$$

In addition to determining the residuals, SaTool can analyse various structural properties of the system and the residuals. Table 2 shows the structural isolability and detectability for the residuals found. Faults on all actuators and sensors are structurally detectable, but several are not structurally isolable. The isolable faults are: the lateral thruster,the position measurements in the horizontal plane, $x_m$ and $y_m$, the heading measurement $\psi_m$ and the

turn rate measurement $r_m$. While structural isolability is

Table 2. Structural detectability and isolability of Minerva achieved from a ranking algorithm

|  | $a_1$ | $a_2$ | $a_3$ | $a_4$ | $m_1$ | $m_2$ | $m_3$ | $m_4$ | $m_5$ | $m_6$ | $m_7$ |
|---|---|---|---|---|---|---|---|---|---|---|---|
| $d/i$ | $d$ | $d$ | $i$ | $d$ | $i$ | $i$ | $d$ | $i$ | $d$ | $d$ | $i$ |

not achievable for some of the sensor and thruster failures using these residuals it is possible to isolate more failures when extending the isolation strategy. Thruster failures are only present in $r_{4-7}$ and can be isolated from each other by considering the sign of the residuals. The signed mapping from thruster faults to residuals is,

$$\begin{pmatrix} r_4 \\ r_5 \\ r_6 \\ r_7 \end{pmatrix} \leftarrow \begin{array}{c} \begin{array}{cccc} u_1 & u_2 & u_3 & u_4 \end{array} \\ \begin{pmatrix} 0 & 0 & 0 & 1 \\ 1 & 1 & 0 & 0 \\ 1 & -1 & 1 & 0 \\ -1 & 1 & 1 & 0 \end{pmatrix} \end{array} \tag{12}$$

Using (12) thruster fault can be isolated through column matching with the signature observed in the residuals.

Enhanced isolation can also be obtained using an algorithm [Krysander et al., 2008] to find all minimal structurally overdetermined (MSO) subsets of the system. An MSO set contains only one constraint more than variables in the subgraph of the system to which the variables and constraints belong.

The MSO set algorithm and other general matching algorithms can make it possible to obtain enhanced structural isolability by using a larger set of residuals than the one obtained from a single matching. This implies added complexity associated with having to calculate a larger number of residuals in parallel. A selection method for the relevant MSO sets from a large number of available sets is therefore of convenience.

The MSO sets for the Minerva system in Table 1 yields 483 MSO sets. It is neither feasible nor necessary to implement all of these. A desired structural isolability can be obtained by only a slight increase in number of parallel calculated residuals. This is shown in Table 3.

Table 3. Structural detectability and isolability of Minerva achieved from MSO sets

|  | $a_1$ | $a_2$ | $a_3$ | $a_4$ | $m_1$ | $m_2$ | $m_3$ | $m_4$ | $m_5$ | $m_6$ | $m_7$ |
|---|---|---|---|---|---|---|---|---|---|---|---|
| $d/i/n$ | $i$ | $i$ | $i$ | $d$ | $i$ | $i$ | $d$ | $i$ | $i$ | $i$ | $i$ |

An algorithm to select MSO sets to optimise isolability while also considering computational complexity was presented in [Svärd et al., 2011]. Using this approach, the MSO sets that provide the largest utility to a given objective is selected in each of several iterations. Eq. (13) describes a *utility function* $\mu_{\mathcal{I}}(S)$

$$\mu_{\mathcal{I}}(S) = |\ \sigma_{\mathcal{I}}(\{S\})\ |, \tag{13}$$
$$\sigma_{\mathcal{I}}(\mathcal{M}) = \{I \in \mathcal{I} : \exists S \in \mathcal{M}, S \in I\}, \tag{14}$$

where $S$ is an MSO set, $I$ is an isolation class describing which MSO set will provide isolability of faults by hypothesis test on the elements of the residual vector. With $\mathcal{I}$ being the set of all isolation classes and $\mathcal{M}$ the set of candidate MSO sets that make up the solution, $\sigma_{\mathcal{I}}(\mathcal{M})$, (14) , describes which isolation classes are covered by the candidate MSO sets. For a complete solution $\sigma_{\mathcal{I}}(\mathcal{M}) = \mathcal{I}$.

Table 1. System constraints for ROV Minerva displayed as they are automatically generated by SaTool. The parameters $D_i$ and $M_{A,i}$ indicate damping and added mass terms respectively.

| | | | |
|---|---|---|---|
| $a_1$ | $\tau_1 = g_p(u_1)$ | $m_5$ | $u_m = u$ |
| $a_2$ | $\tau_2 = g_s(u_2)$ | $m_6$ | $v_m = v$ |
| $a_3$ | $\tau_3 = g_l(u_3)$ | $m_7$ | $r_m = r$ |
| $a_4$ | $\tau_4 = g_v(u_4)$ | $m_8$ | $\hat{u}_c = u_c$ |
| $d_1$ | $\dot{x} = \frac{d}{dt}x$ | $m_9$ | $\hat{v}_c = v_c$ |
| $d_2$ | $\dot{y} = \frac{d}{dt}y$ | $m_{10}$ | $\hat{w}_c = w_c$ |
| $d_3$ | $\dot{z} = \frac{d}{dt}z$ | $c_1$ | $X = \tau_1 \cos(\alpha_p) + \tau_2 \cos(\alpha_s)$ |
| $d_4$ | $\dot{\psi} = \frac{d}{dt}\psi$ | $c_2$ | $Y = \tau_3 + \tau_1 \sin(\alpha_p) + \tau_2 \sin(\alpha_s)$ |
| $d_5$ | $\dot{u} = \frac{d}{dt}u$ | $c_3$ | $Z = \tau_4$ |
| $d_6$ | $\dot{v} = \frac{d}{dt}v$ | $c_4$ | $N = \tau_3\, xl - \tau_1\,(y_p \cos(\alpha_p) - x_p \sin(\alpha_p)) - \tau_2\,(y_s \cos(\alpha_s) - x_s \sin(\alpha_s))$ |
| $d_7$ | $\dot{w} = \frac{d}{dt}w$ | $c_5$ | $\dot{\psi} = r$ |
| $d_8$ | $\dot{r} = \frac{d}{dt}r$ | $c_6$ | $\dot{x} = u \cos(\psi) - v \sin(\psi)$ |
| $d_9$ | $\dot{u}_c = \frac{d}{dt}u_c$ | $c_7$ | $\dot{y} = v \cos(\psi) + u \sin(\psi)$ |
| $d_{10}$ | $\dot{v}_c = \frac{d}{dt}v_c$ | $c_8$ | $\dot{z} = w$ |
| $d_{11}$ | $\dot{w}_c = \frac{d}{dt}w_c$ | $c_9$ | $\dot{u}\, m = X - D_1(u - u_c)(u - u_c) - M_{A,1}(\dot{u} - \dot{u}_c) - M_{A,26}\, r^2 + m\, r\, v + M_{A,2}\, r\,(v - v_c)$ |
| $m_1$ | $x_m = x$ | $c_{10}$ | $\dot{v}\, m = Y - D_2(v - v_c)(v - v_c) - \dot{r}\, M_{A,26} - M_{A,2}(\dot{v} - \dot{v}_c) - m\, r\, u - M_{A,1}\, r\,(u - u_c)$ |
| $m_2$ | $y_m = y$ | $c_{11}$ | $\dot{w}\, m = Z - D_3(w - w_c)(w - w_c) - M_{A,3}(\dot{w} - \dot{w}_c) + W - B$ |
| $m_3$ | $z_m = z$ | $c_{12}$ | $I_z\, \dot{r} = N - \dot{r}\, M_{A,6} - M_{A,62}(\dot{v} - \dot{v}_c) - r\, D_6(r) + (M_{A,1} - M_{A,2})(u - u_c)(v - v_c) - M_{A,26}\, r\,(u - u_c)$ |
| $m_4$ | $\psi_m = \psi$ | | |

If more than one MSO set provides the highest utility the one with the lowest cardinality is selected. Iteration is continuer until a complete solution has been found or all MSO sets have been evaluated. The algorithm evaluates the realizability of residuals using the MSO sets and use only realizable residuals, see [Svärd et al., 2011]. Using such selection, desired isolability is obtained with only 6 residuals listed in (15). Faults in velocities $u_m$ and $v_m$, that both origin from the Doppler Log are group-wise but not individually isolable.

$$
\begin{pmatrix} r_1 \\ r_2 \\ r_3 \\ r_4 \\ r_5 \\ r_6 \end{pmatrix} \leftarrow
\begin{array}{ccccccccccc}
u_1 & u_2 & u_3 & u_4 & x_m & y_m & z_m & \psi_m & u_m & v_m & r_m \\
0 & 0 & 0 & 0 & 1 & 0 & 0 & 1 & 1 & 1 & 0 \\
0 & 0 & 0 & 0 & 0 & 1 & 0 & 1 & 1 & 1 & 0 \\
0 & 0 & 0 & 0 & 0 & 0 & 0 & 1 & 0 & 0 & 1 \\
0 & 0 & 0 & 1 & 0 & 0 & 1 & 0 & 0 & 0 & 0 \\
1 & 0 & 1 & 0 & 0 & 0 & 0 & 0 & 1 & 1 & 1 \\
1 & 1 & 0 & 0 & 0 & 0 & 0 & 0 & 1 & 1 & 1
\end{array}
\tag{15}
$$

It is noted that $r_{1-4}$ are functionally identical to the residuals obtained through the ranking algorithm.

While the increased structural isolability is advantageous it is outweighed for this particular system by the additional complexity introduced through generating additional residuals. Applying the isolability strategy in to include signatures of faults, Eq. 12, provides the desired isolability and this approach will be used subsequently.

Due to the fact that the estimate of the ocean current is based on a dynamical model of the vessel, faults in the actuators and sensors will compromise the current estimate. As the current is used in the residuals the ocean current observer is halted when a fault is detected and the previous ocean current estimates in the inertial frame from when the vessel was fault free are used. Under the assumption of a slowly-varying current this approach is reasonable. Additionally it is necessary to assume that no faults occur during the start-up of the UUV until all sensors and thrusters have been initialized.

## 4. CHANGE DETECTION

Fault detection is achieved through change detection applied to residuals. A standard *Generalised Likelihood Ratio Test* (GLRT) algorithm for Gaussian residuals with independent discrete-time observations will be used, even though this assumption will be violated for real data. With $\theta$ being system parameters, $\theta_0$ denotes the normal ($\mathcal{H}_0$) and $\theta_1$ the faulty system ($\mathcal{H}_1$). The log-likelihood ratio

$$
s(r) = \ln \frac{p(r; \hat{\theta}_1)}{p(r; \hat{\theta}_0)},
\tag{16}
$$

is used in GLRT algorithm to provide the test statistic,

$$
g(k) = \max_{k-M+1 \le j \le k} \max_{\theta_1} \sum_{i=j}^{k} s(r(i))
\tag{17}
$$

where $k$ is the current time, $j$ the fault occurrence time and $M$ is algorithm window size. A fault is detected when $g(k)$ exceeds a threshold $h$ and the fault occurrence time $\hat{k}_0$ and change magnitude $\hat{\theta}_1$ is computed from,

$$
(\hat{k}_0, \hat{\theta}_1) = \arg\left\{ \max_{1 \le j \le k} \max_{\theta_1} S_j^k(\theta_1) \right\}.
\tag{18}
$$

The implementation of (16),(17), and (18) is done here using the condition that faults are strongly detectable [Blanke et al., 2006]. This is the case for the additive faults. For multiplicative faults, i.e. thruster gains, this is the case when sea current is nonzero or some manoeuvring takes place.

Theoretical calculation of thresholds $h$ is straightforward when signals are independent and identically distributed (IID) and their distributions are Gaussian. When distributions are non-gaussian, a theoretic threshold may not be calculable by analytical means. As an alternative, [Blanke et al., 2012] and [Galeazzi et al., 2012] suggested that thresholds are estimated from data. The distribution of $g(k)$ for the healthy system is estimated and $h$ is determined to give a desired false alarm probability. This method was further elaborated and applied to an unmanned aerial vehicle in [Hansen and Blanke, 2014] and a similar method is used in this paper using sea trial data.

## 5. SIMULATION RESULTS

The fault diagnosis has been investigated by simulation of the mathematical model described in Section 2. White Gaussian noise with zero mean and variance $\sigma^2 = 10^{-6}$ have been applied to the sensors and the vessel is subject to a constant ocean current of $\mathbf{v}_c = [-0.2\,\frac{m}{s}, 0.2\,\frac{m}{s}, 0.2\,\frac{m}{s}]^T$ in the inertial frame. Two thruster failure cases were considered:

*Complete thruster failure.* During station-keeping in the presence of ocean current the starboard-side horizontal thruster $u_2$ suddenly experiences a failure reducing its produced thrust to zero. The residuals are shown on Fig. 3.
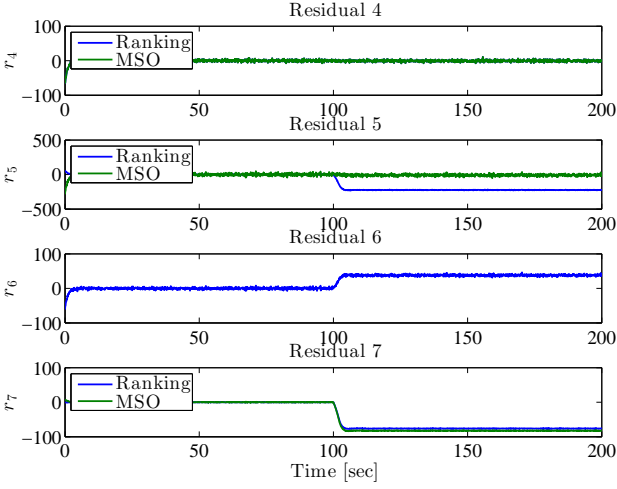


Fig. 3. Residuals during thruster failure. Fault occurs at time $t = 100s$. Blue color lines are residuals obtained using the ranking algorithm, green are MSO sets residuals. $r_{1-4}$ are functionally identical for the two methods.

After the occurrence of the fault at time $t = 100s$ residuals $r_5, r_6, r_7$ clearly deviate from zero while $r_4$ is unaffected. The residuals generated with the MSO set method enable direct isolation as only one residual is affected by the fault. The MSO set residuals are obtainable as combinations of analytical redundancy relations obtained by other matching algorithms but the MSO set algorithm is by far the faster way to obtain these. Detectability properties are equivalent for the algorithms, but using a richer set of residuals, as in the MSO approach, most often enhances isolability.

As an example, Figure 4 illustrates how, using the GLRT algorithm, a fault is detected and the fault signature is used to isolate which thruster has a fault.

*Loss of thruster effectiveness.* During station-keeping $u_2$ suffers a parametric fault such that obtained thrust is down to 25% of thrust desired. The resulting residuals are shown in Fig. 5.

Using the GLRT estimate of the fault magnitude it is possible to estimate the effectiveness of the thruster after the faults has occurred. The fault magnitude of residuals $r_{4-7}$ is an estimate of

$$\hat{\boldsymbol{\mu}}_1 = \mathbf{F}_{expected} - \mathbf{F}_{observed}, \qquad (19)$$
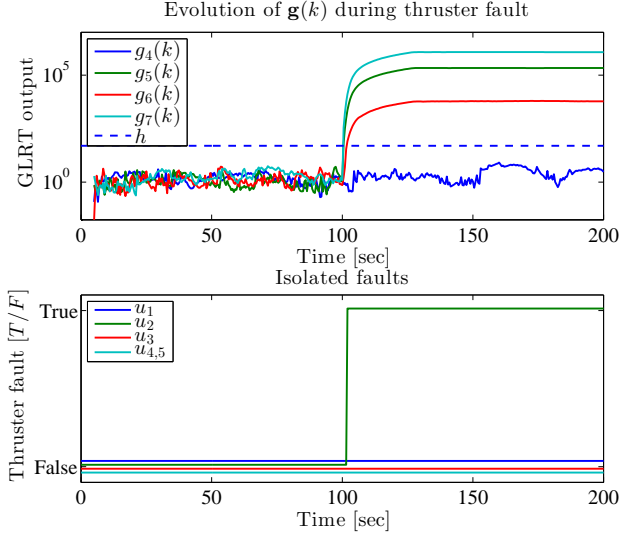


Fig. 4. GLRT output during thruster failure. Fault occurs at time $t = 100s$. The fault is correctly isolated as $u_2$.
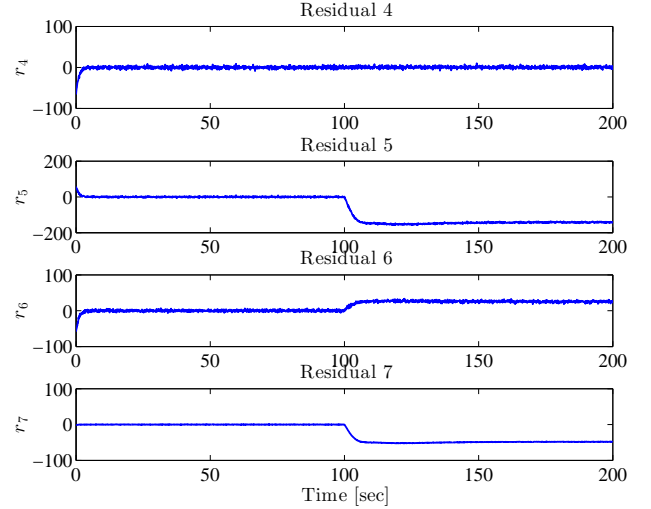


Fig. 5. Residuals during thruster degradation. Fault occurs at time $t = 100s$.

where $\mathbf{F}_{expected}$ is the expected induced forces and moments from the thrusters and $\mathbf{F}_{observed}$ is the observation from the measurements. An estimate of the parametric fault on $u_2$ using (19) is shown in Fig. 6 together with the GLRT output.

## 6. SEA TRIAL RESULTS

By courtesy of Zhao Bo from NTNU [Zhao et al., 2012], [Zhao et al., 2014] recorded data from sea trials have been made available for analysis. Faults on sensors were induced and can be used to verify the methods discussed in this paper. The residuals $r_1, r_2$ are shown on Fig. 7 where a bias on the doppler velocity log has been applied.

To detect the fault an appropriate threshold $h$ is found using data of fault-free operation. Using the approach of [Hansen and Blanke, 2014] a Weibull distribution, (20), is used to fit the test statistics.

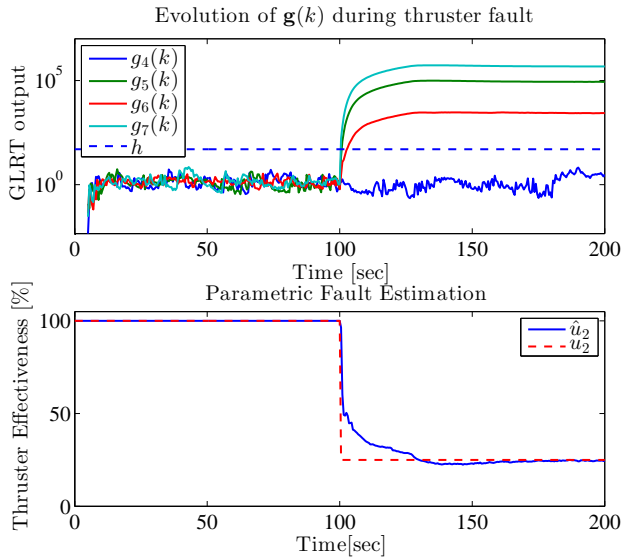$$P(x; \alpha, \beta) = 1 - e^{(x/\alpha)^\beta} \qquad (20)$$

Fig. 6. GLRT output during thruster degradation. Fault occurs at time $t = 100s$. An estimate of the thruster effectiveness is also shown.
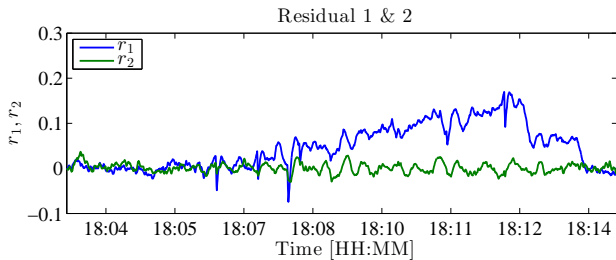


Fig. 7. Residuals during DVL drift.

The scale $\alpha$ and shape $\beta$ parameters are estimated using a maximum likelihood method. Fig. 8 shows a probability plot of the GLRT output and the fitted distribution.

The threshold $h$ for the GLRT is determined from the estimated weibull distribution based on a false alarm probability $P_{FA}$ using, (21).

$$h = \alpha(-\ln(P_{FA}))^{\frac{1}{\beta}} \tag{21}$$



Fig. 8. Probabillity plot of the GLRT decision function in the no-fault case.

Based on the fit shown in Fig. 8 a desired $P_{FA} = 0.01\%$ per hour would result in a threshold of $h = 47.3$. The chance to detect a fault $P_D$ is more difficult to estimate since the amount of data $\mathcal{H}_1$ data is limited. The approach is the same as for the no fault case except a *generalized extreme value* (GEV) distribution [Coles, 2001] is used to fit the GLRT as this provides a closer fit. The GEV distribution has the cumulative distribution function (22)

$$P(x; k, \sigma, \mu) = e^{-(1+k(\frac{x-\mu}{\sigma}))^{-1/k}}, \tag{22}$$

where $\mu$, $\sigma$, and $k$ are the location, scale and shape respectively. The corresponding probability plot is shown on Fig. 9. The fit only roughly describes the distribution of the test statistic so the chance to detect will be quite uncertain. Using the fit shown gives $P_D = 94\%$.
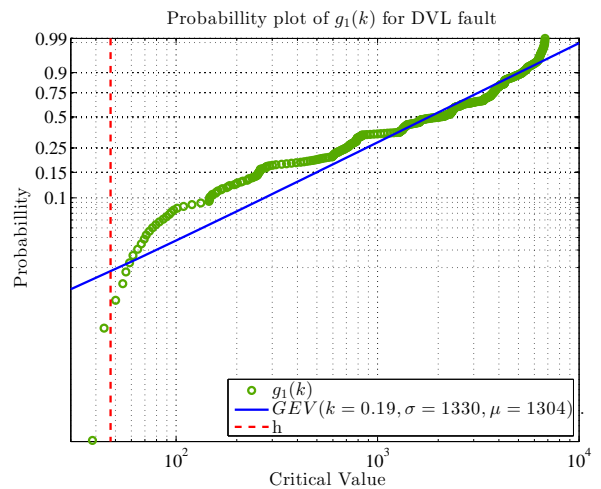


Fig. 9. Probabillity plot of the decision function after a fault has occurred on the doppler log.

Fault magnitudes are estimated via the GLRT estimate of $\hat{\mu}_1$. This is in particular relevant for additive faults, such as DVL bias, because it allows for straightforward fault compensation. Fig. 10 shows the GLRT decision function and the fault magnitude estimate. While there is a clear deviation between the estimated fault magnitude and the actual induced bias the estimate gives a reasonable indication and could conceivably be used for accommodation of the fault.

## 7. CONCLUSIONS

Fault diagnosis for an underwater ROV was considered in this paper. Diagnosis was performed using structural analysis for residual generation and the GLRT algorithm for hypothesis testing. Structural analysis was found convenient because tools exist that performs the analysis and derives the relevant residuals automatically. Both a simple ranking algorithm and a more sophisticated approach with selection of MSO sets were investigated and fault isolability properties were highlighted. It was demonstrated how thresholds for the GLRT algorithm could be determined using data from fault-free operation with the aim of obtaining a low probability of false alarms. The diagnosis algorithms were tested using both numerical simulations and measurement data from sea trials that both confirmed the efficacy of the approach.
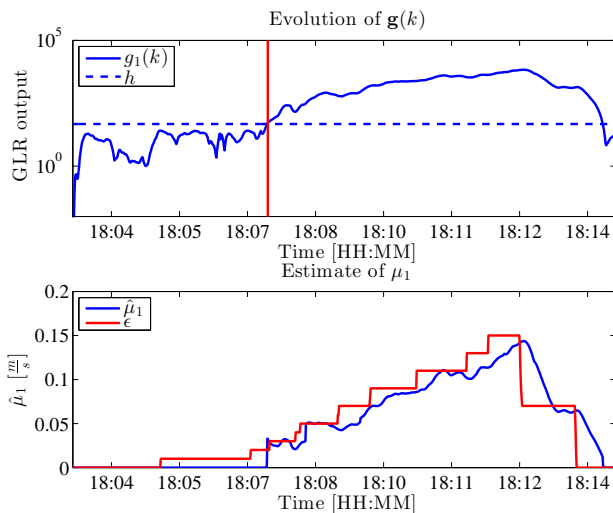
Fig. 10. Results of the change detection algorithm used on residual 1: GLR output $g_1(k)$; estimated fault magnitude $\hat{\mu}_1$ and actual bias.

## ACKNOWLEDGEMENTS

## REFERENCES

A. Alessandri, M. Caccia, and G. Veruggio. Fault detection of actuator faults in unmanned underwater vehicles. *Control Engineering Practice*, 7(3):357–368, 1999.

Gianluca Antonelli. Four fault Detection/Tolerance strategies for AUVs and ROVs. In *Underwater Robots $2^{nd}$ Edition*, number 2 in Springer Tracts in Advanced Robotics, 79–91. Springer, 2006.

M. Blanke. Diagnosis and fault-tolerant control for ship station keeping. In *Proc. of the 2005 IEEE Mediterranean Conf. on Control and Automation*, 1379 –1384, 2005.

M. Blanke, S. Fang, and R. Galeazzi. B. J. Leira. Statistical change detection for diagnosis of buoyancy element defects on moored floating vessels. In *Proc. $8^{th}$ IFAC SAFEPROCESS*, 462–467, 2012.

M. Blanke and T. Lorentzen. SaTool - a software tool for structural analysis of complex automation systems. In *Proc. $6^{th}$ IFAC SAFEPROCESS*, 673–678, 2006.

M. Blanke, M. Kinnaert, J. Lunze, and M. Staroswiecki. *Diagnosis and Fault-Tolerant Control*. 2.ed, Springer, 2006.

E. Børhaug, L. Pivano, K. Y. Pettersen, and T. A. Johansen. A model-based ocean current observer for 6DOF underwater vehicles. In Zoran Vukic and Sauro Longi, editors, *Proc. IFAC Conf. on Control Applications in Marine Systems (CAMS'2007)*, 169–174, 2007.

S. Coles. *An Introduction to Statistical Modeling of Extreme Values*. Springer, 2001. ISBN 9781852334598.

Maria Letizia Corradini and Giuseppe Orlando. A robust observer-based fault tolerant control scheme for under-water vehicles. *J. of Dynamical Systems, Measurement and Control*, 136(3), 2014. doi: 10.1115/1.4026328.

M.L. Corradini, A. Monteriu, and G. Orlando. An actuator failure tolerant control scheme for an underwater remotely operated vehicle. *IEEE Trans. Control Systems Technology*, 19(5):1036 –1046, September 2011.

F. Dukan, M. Ludvigsen, and A.J. Sorensen. Dynamic positioning system for a small size ROV with experimental results. In *IEEE OCEANS'2011*, 1–10, 2011.

B. Ferreira, A. Matos, and N. Cruz. Automatic reconfiguration and control of the MARES AUV in the presence of a thruster fault. In *OCEANS, 2011 IEEE - Spain*, 1–8, 2011.

T. I. Fossen. *Marine Control Systems: Guidance, Navigation and Control of Ships, Rigs and Underwater Vehicles*. Marine Cybernetics, 2002.

T. I. Fossen. *Handbook of Marine Craft Hydrodynamics and Motion Control*. John Wiley & Sons, 2011.

R. Galeazzi, M. Blanke, and N. K. Poulsen. Detection of parametric roll for ships. In *Parametric Resonance in Dynamical Systems*, 17–43. Springer, 2012.

G. Griffiths and A. Trembanis. Towards a risk management process for autonomous underwater vehicles. *Masterclass in AUV technology for polar science*, 103–118, 2007.

Søren Hansen and Mogens Blanke. Diagnosis of airspeed measurement faults for unmanned aerial vehicles. *IEEE Trans. Aerospace and Electronic Systems*, 50 (1), 2014.

M. Kirkeby. Comparison of Controllers for Dynamic Positioning and Tracking of ROV Minerva. Dept. of Marine Technology, NTNU, Trondheim, Norway, 2010.

M. Krysander, J. Aslund, and M. Nyberg. An efficient algorithm for finding minimal overconstrained subsystems for model-based diagnosis. *IEEE Trans. Systems, Man and Cybernetics*, 38(1):197–206, 2008.

Q. Liu, D. Zhu, and S. X. Yang. Unmanned underwater vehicles fault identification and fault-tolerant control method based on FCA-CMAC neural networks, applied on an actuated vehicle. *J. of Intelligent & Robotic Systems*, 66(4):463–475, 2012.

Edin Omerdic and Geoff Roberts. Thruster fault diagnosis and accommodation for open-frame underwater vehicles. *Control Engineering Practice*, 12(12):1575–1598, 2004.

A. J. Sørensen, F. Dukan, M. Ludvigsen, D. A. Fernandez, and M. Candeloro. Development of dynamic positioning and tracking system for the ROV minerva. In *Further Advances in Unmanned Marine Vehicles*, 113–128. IET, 2012.

C. Svärd, M. Nyberg, and E. Frisk. A greedy approach for selection of residual generators. In *Proc. 22. Int. Workshop on Principles of Diagnosis (DX-11)*, 2011.

H.-P. Wolf and M. Blanke. Satool - a set of tools for structural analysis Dept. of Electrical Engineering, Technical University of Denmark, 2014.

B. Zhao, M. Blanke, and R. Skjetne. Particle filter based fault-tolerant ROV navigation using hydro-acoustic position and doppler velocity measurements. In *9th IFAC Int. Conf. on Manoeuvring and Control of Marine Craft, MCMC*, 2012.

B. Zhao, R. Skjetne, M. Blanke, and F. Dukan. Particle filter for fault diagnosis and robust navigation of underwater robot. *IEEE Trans. Control Systems Technology*, 2014.